Accepted Manuscript

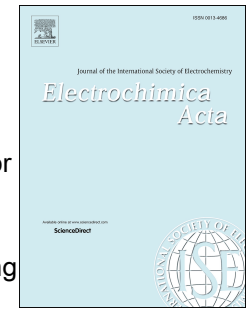

Phenothiazine dye featuring encapsulated insulated molecular wire as auxiliary donor for high photovoltage of dye-sensitized solar cells by suppression of aggregation

Tao Hua, Zu-Sheng Huang, Ke Cai, Lingyun Wang, Hao Tang, Herbert Meier, Derong Cao

PII: S0013-4686(19)30239-7

DOI: https://doi.org/10.1016/j.electacta.2019.02.013

Reference: EA 33604

To appear in: *Electrochimica Acta*

Received Date: 10 December 2018

Revised Date: 3 February 2019

Accepted Date: 3 February 2019

Please cite this article as: T. Hua, Z.-S. Huang, K. Cai, L. Wang, H. Tang, H. Meier, D. Cao, Phenothiazine dye featuring encapsulated insulated molecular wire as auxiliary donor for high photovoltage of dye-sensitized solar cells by suppression of aggregation, *Electrochimica Acta* (2019), doi: https://doi.org/10.1016/j.electacta.2019.02.013.

Phenothiazine Dye Featuring Encapsulated Insulated Molecular Wire as Auxiliary Donor for High Photovoltage of Dye-Sensitized Solar Cells by Suppression of Aggregation

Tao Hua [a], Zu-Sheng Huang[b], Ke Cai[a], Lingyun Wang[a], Hao Tang[a], Herbert Meier* [a,c] and Derong Cao*[a]

[a] *State key Laboratory of Luminescent Materials and Devices, School of Chemistry and Chemical Engineering, South China University of Technology, Guangzhou 510641, China*

[b] *School of Pharmaceutical Sciences, Wenzhou Medical University, Wenzhou 325035, China*

[c] *Institute of Organic Chemistry, University of Mainz, Mainz 55099, Germany*

*Corresponding author. E-mail: drcao@scut.edu.cn (D. Cao), hmeier@uni-mainz.de (H. Meier)

ABSTRACT

Two efficient dye-sensitized solar cells have been fabricated by two novel D–D–π–A phenothiazine-based organic dyes (**PH2** and **PH3**) with an encapsulated insulated molecular wire (EIMW) as an auxiliary donor. The cell sensitized by **PH2** with EIMW as an auxiliary donor shows a much higher photovoltage (V_{oc}) relative to the reference dye **PH1** without EIMW, because the former dye can inhibit dye aggregation and suppress the charge recombination effectively. The results show that the cell sensitized by **PH2** with co-adsorption of chenodeoxycholic acid obtains a high power conversion efficiency, even higher than that of the cell based on **N719**. Thus, an effective way to increase the photovoltage and efficiency of the DSSCs has been developed by introducing the EIMW into the organic dyes due to the effective inhibition of dye aggregation and charge recombination.

Keywords: encapsulated insulated molecular wire; dye-sensitized solar cells; auxiliary donor; suppression aggregation

1. Introduction

Dye-sensitized solar cells (DSSCs) have attracted considerable attention from both academic and industrial research communities in the past 25 years, because of their favorable ecological feature, economical characteristic and ease to tune various structural characters [1-8]. Although a variety of photovoltaic materials have been concerned, such as perovskites [9,10], organic small molecules, polymers [11-13] and quantum dots solar cells. However, Dye-sensitized solar cells still play an important role in striving towards the next generation solar technology due to their flexible structure modification and superior performance. Up to now, power conversion efficiencies (PCEs) of dye-sensitized solar cells have exceeded 13% [14,15]. The enormous efficiency breakthrough of DSSCs has been greatly benefited from new materials design and device engineering, including the use of donor–donor–π spacer–acceptor (D–D–π–A) architectures [16-20], the larger plane structure [4,21], the effectively π–spacer [22-24], co-adsorption [25,26] or co-sensitization [27-30], amendment of the interfacial morphology of TiO_2 [31-42], reform of the electrolyte composition [43-47], and so on.

Phenothiazine dyes were one class of the most attractive metal-free dyes in the past few years because the phenothiazine units possess strong electron-donating ability and non-planar butterfly conformation [48-51]. Besides, phenothiazine unit can be modified easily with a considerable efficiency simultaneously. Recent research

found that introducing an auxiliary donor at the terminal of phenothiazine unit could effectively improve the PCE of the dyes [52-57]. Zhu et al reported a series of phenothiazine-based dyes by introducing thiophene and ethylenedioxythiophene, their dimers and the mixtures of the both to adjust dye aggregation, suppress charge recombination and improve dye regeneration. The results show that thiophene analogues as auxiliary donors not only improve light adsorption property and adjust energy levels, but also have an effect on dye aggregation and interfacial charge recombination [58].

At present, a majority of organic sensitizers are provided of donor, π–spacer, and acceptor (D–π–A configuration) and most of them possess rigid rod-shaped skeleton [59-61]. However, the rigid rod-shaped skeletons of dyes are easily generated intermolecular aggregation and charge recombination on the surface of TiO_2 [62-66]. The two negative effects not only accelerate the process of self-quenching of generated electron and cut down the electron injection into TiO_2, but also reduce the stability of these dyes. In addition, aggregation and charge recombination of organic dye on the surface of TiO_2 also restrict the improvement of the J_{sc} and V_{oc}. At present, the main strategies to restrain intermolecular aggregation and charge recombination of the sensitizers are introducing alkyl chain [67-69], and bulky group [70-72] or co-sensitization [73,74], and so on. But these tactics do not show obvious effect on the two negative aspect sometimes, such as the triiodide can easily penetrate through the alkyl chain or the interval to reach the surface of TiO_2 [75].

Therefore, a more effective method is highly desired, which not only can prevent

the redox couple approach of the surface of TiO_2, but also can suppress the intermolecular aggregation. For example, introducing a more appropriate group into the ordinary dyes at an appropriate site could form a compact sensitizer layer at the surface of the TiO_2. Rotaxane has attracted considerable attention in the recent years because of specific framework consisting of mechanically interlocked threads and macrocycles, which has remarkable potential to evolve into molecular switches and multifunctional rotaxane-based molecular systems in future [76-78]. Introducing the rotaxane-like molecule into the DSSCs at an appropriate site, not only suppress the dye aggregation and reduce the charge recombination, but also immobilizes the conjugated backbone in a planar configuration [79]. Encapsulated insulated molecular wire (EIMW) is a rotaxane-like configuration which may play a role as a barrier between the two dye molecules. Pyrene is a polycylic aromatic hydrocarbon which has extensive electron delocalization nature [80,81]. It could be exploited as a sensitization unit by coupling with electron rich moieties [82]. Thus, introducing the pyrene into the donor of PTZ may enhance the light absorption capacity, meanwhile, introducing the EIMW unit into the system may suppress dye aggregation.

Based on the above considerations, two novel phenothiazine dyes (**PH2** and **PH3**) with EIMW as an auxiliary donor were designed and synthesized (Fig. 1). To the best of our knowledge, EIMW unit is introduced as the auxiliary donor into the organic dyes for the first time. **PH1** without EIMW was prepared as a reference dye. The photophysical, electrochemical and photovoltaic properties of the dyes and their DSSCs were studied systematically.

Fig. 1. Chemical structures of the sensitizers (**PH1**, **PH2** and **PH3**).

2. Experiment

2.1 Materials and Reagents

The raw materials were purchased from J&K, Energy Chemical and Adamas in analytical grade. Toluene, THF, dioxane and 1,2-dichloroethane were distilled by sodium. Other solvents and regents were of an analytical grade and used without further purification. The reactions were monitored by TCL until the reaction completely. Chromatographic separations were carried out on silica gel (300-400 mesh).

2.2 Instruments and Characterization

^{1}H and ^{13}C NMR spectra were recorded on Bruker 400 MHz instrument in $CDCl_3$, DMSO-d_6 and THF-d_8. HRMS spectra were recorded on an Agilent Technologies 1290 Infinity mass spectrophotometer. Melting point was measured on SGW X-4B microscopic melting point apparatus. Ultraviolet-Visible (UV-Vis) spectra of the dyes in solution were recorded on a Shimadzu UV-2450 spectrophotometer. Ultraviolet-Visible (UV-Vis) spectra of the dyes anchored on TiO_2 film were recorded on a UV-3010 spectrophotometer. The PL spectra were recorded on a Fluorolog III photoluminescence spectrometer. Electrochemical redox potentials were performed by cyclic voltammetry (CV) using a three electrode cell on an electrochemistry workstation at a scan rate of 50 mV s^{-1}. The dye adsorbed on TiO_2 films were used as a working electrode. A platinum wire was utilized as the counter electrode and Ag/AgCl (0.01 M) as reference electrode. Tetrabutylammonium hexafluorophosphate

($TBAPF_6$, 0.1 M in dry acetonitrile) was used as the supporting electrolyte. The ferrocene/ferrocenium (Fc/Fc^+) redox couple acts as an internal potential. The incident monochromatic photon-to-current conversion efficiency (IPCE) spectra were achieved on a Spectral products DK240 monochromator from the 300~800 nm region. The current-voltage characteristics were recorded on a Keithley 2400 source meter under simulated AM 1.5G (100 mW cm^{-2}) illumination with a standard solar light simulator with a mask. The electrochemical impedance spectra (EIS) were recorded on a Zahner Zennium electrochemical workstation under dark conditions.

2.3 Fabrication of dye-sensitized solar cells

The fabrication of the cell was carried out according to the reported procedures [83-85]. Fluorine-doped tin oxide (FTO) glasses were washed with water, ethanol and acetone in an ultrasonic bath to remove impurity. TiO_2 nanoparticles (10 nm) were prepared by a hydrothermal treatment with a precursor solution containing 5 mL $Ti(OBu)_4$, 10 mL ethanol, 9 mL acetic acid and 25 mL deionized water. The TiO_2 powder (0.5 g) was ground for 40 min in the mixture of 4.0 mL ethanol, 0.1 mL acetic acid, 1.5 g terpineol and 0.25 g ethyl cellulose to achieve a homogeneous suspension. Finally, the plup suspension was sonicated for 20 min in an ultrasonic bath to produce a viscous white TiO_2 sizing agent. The TiO_2 photoanodes were prepared by the screen-printing process on FTO glass, the thickness of the TiO_2 photoanode films was controlled about 16 μm (12 μm thick transparent layer and 4 μm thick scattering layer). The prepared films were annealed through a temperature programming. The main program as follow: 325 ^oC for 5 min, 375 ^oC for 5 min, 450 ^oC for 15 min, and

500 ^{o}C for 15 min then cooling to room temperature. The TiO_2 films were treated by 0.04 M $TiCl_4$ aqueous solution for 30 min at 70 ^{o}C to improve photovoltaic performance. Then TiO_2 films were rinsed with deionized ethanol and water, then sintered again at 520 ^{o}C for 30 min. After the films cooling to room temperature, the films were immersed in a 3.0×10^{-4} M solution of the dyes for 24 h (The solution is a mixture solvent of acetonitrile and tert-butanol (volume ratio of 1:1) at 25 °C [86]. For the co-adsorption, chenodeoxycholic acid was added into the dye solution at a concentration of 1 mM. Afterward these films were washed with ethanol and dried naturally. The dye-loaded TiO_2/FTO glass films were assembled into a sandwiched type together with a Pt/FTO counter electrode. The active area of the dye coated TiO_2 film was 0.16 cm^2.

Scheme 1. Synthesis routes of dyes **PH1−3**.

3. Results and Discussion

3.1 Synthesis

Compounds **4** and **12** were synthesized according to the references [87-89]. Compound **14** was conveniently obtained by Suzuki coupling reaction from compound **13** and compound **6**, then compound **14** was hydrolyzed with CF_3COOH to give the target product **PH2**. Compound **15** was synthesized by NBS with **14**. **PH3** was obtained through a similar hydrolysis reaction to that of **PH2**. All new compounds were characterized by multiple spectroscopic tools (NMR, HRMS). The synthesis route of the dyes **PH1–3** is depicted in Scheme 1.

3.2 Spectroscopic studies

The UV-Vis absorption spectra of **PH1**, **PH2** and **PH3** were recorded in CH_2Cl_2 (Fig.

2a), and the detailed data are summarized in Table 1. The three dyes have two major broad absorption bands in the range of 300−650 nm. The high-energy bands located at 300−400 nm are due to localized aromatic π–π* electronic transition of the chromophores; the low-energy bands located at 420−650 nm are ascribed to intramolecular charge transfer (ICT) from the donor to the acceptor. The maximum absorption wavelengths of **PH1**, **PH2** and **PH3** are 493, 506 and 508 nm, respectively. In comparison with **PH1**, the λ_{max} of **PH2** displays a red-shift of 12 nm due to a more coplanar configuration by EIMW unit. The rigid circle chain fixes the bithiophene in a coplanar configuration, which increases the probability of the ICT transition from the donor to the acceptor. This appearance can be verified in the later by the DFT calculation. It is surprised that **PH3** only has a 2 nm red-shift relative to **PH2**. Interestingly, an additional shoulder peak appears in the UV-Vis absorption spectra of the three dyes, which is according to the additional π–π* electron transitions due to introducing the additional donor and the peaks became more obvious follow with the planarity of the molecule improving. The molar extinction coefficients for **PH1**, **PH2** and **PH3** are 2.15×10^4, 2.39×10^4 and 2.89×10^4 $M^{-1}cm^{-1}$, respectively. **PH2** and **PH3** have higher molar extinction coefficients than **PH1**. When the dyes adsorbed on TiO_2, all of the absorption spectra are broadened. The maximum absorption of **PH1** and **PH2** exhibit 27 and 14 nm blue-shift with respect to those in the solution, respectively. The reason of this hypochromatic shift may be ascribed to deprotonation of the carboxylic acid and intermolecular aggregation. **PH2** shows a slight blue-shift although it presents better planarity, which might be due to introducing the EIMW

into the system. Interestingly, **PH3** displays about 40 nm blue-shift. This phenomenon maybe due to introducing the pyrene into the system, which let dye **PH3** has a better planarity, the circle chain could not suppress the aggregation completely.

To understand the origins of the additional absorption band in D–D–π-A dyes, we determined the UV-Vis absorption spectra of the additional donor (bithiophene, EIMW and pyrene), the results are shown in Figure S31. The bithiophene unit and EIMW unit show a shoulder peak at 330 nm and the shoulder peak of the latter more obvious. In addition, pyrene unit shows an absorption peak at 340 nm. While above-mentioned building blocks connect with phenothiazine system, the absorption peaks are red-shift to near 400 nm. Introducing the additional donor to phenothiazine, the dye shows extra absorption peak due to additional electron transition, and the intensity of the absorption is improved along with extending conjugation[58,90]. In addition, the absorption spectra of dyes co-adsorbed CDCA in solution and the cells with electrolyte solution were determined, as shown in Figure S32 and S33. When CDCA was added, the cell sensitized by **PH1** presented obvious red-shift in comparison with the cell without CDCA. The results indicate a higher degree aggregation of dye **PH1** on the TiO_2 films.

Table 1. Photophysical and electrochemical properties of the dyes

Fig. 2. The UV-Vis absorption spectra of these dyes (a) and the absorption spectra of these dyes adsorbed on TiO_2 films (b).

3.3 Electrochemical properties

To evaluate the thermodynamic possibility of electron injection and regeneration

of the three dyes, cyclic voltammograms were recorded on CH_3CN to determine the oxidation potentials (Fig. 3). The oxidation potentials correspond to the HOMOs, and the electrochemical data are summarized in Table 1. The potential was externally calibrated by ferrocenium/ferrocene (Fc^+/Fc) couple and then was calculated versus NHE electrode ($E_{1/2}$ (Fc^+/Fc) = 0.53 V vs Ag/AgCl in our case, and 0.64 V vs NHE) [91]. The HOMO level of **PH1**, **PH2** and **PH3** are 0.94, 0.95 and 1.14 V, respectively. These values are more positive than the I^-/I_3^- redox potential value (0.4 V *vs.* NHE), indicating that the oxidized dyes can be efficiently regenerated by the electrolyte. The $E_{0\text{-}0}$ values are 2.15, 2.16 and 2.24 V, respectively, which are estimated from the intersection of the normalized absorption and emission spectra. The LUMO levels of **PH1**–**PH3** calculated from HOMO – $E_{0\text{-}0}$ are –1.21, –1.21 and –1.10 V, respectively. The values are more negative than the CB level of the TiO_2 (–0.5 V *vs.* NHE), which implies that an efficient electron injection process from the excited dye into the conduction band of TiO_2 can occur for the dyes.

Fig. 3. Cyclic voltammograms (a) and Schematic energy diagram of these dyes (b).

Table 2. The computed energy levels and the spatial distribution of the frontier molecular orbitals of the dyes

3.4 Theoretical calculations

Density function theory (DFT) calculations at the DFT-B3LYP/6-31G level with Gaussian 09 suite of programs were utilized to investigate the electron-density distributions of the three dyes as shown in Table 2. The HOMO levels of **PH1**–**3** are mainly delocalized throughout the bithiophene and phenothiazine rings, the LUMO

orbitals are delocalized in cyanoacetic acid. It can be found that clear variation when introducing the EIMW into the system. When introducing the pyrene group into the conjugation structure, the LUMO orbitals no obvious changed, but the HOMO orbitals delocalized throughout the pyrene group to the p-(hexyloxy)benzoyl group. The electronic properties of the three dyes indicate that such well-separated orbital distribution is conducive to the electron transfer from HOMO to LUMO and benefits for inducing the electron injection from the LUMO into the conduction band of TiO_2.

The optimized ground-state geometries of the three dyes are shown in Table 2. For **PH1**, the dihedral angles between the two thiophenes, thiophene and phenothiazine are 2.87 ^{o} and 18.55 ^{o}, respectively. For **PH2** with EIMW unit linked to bithiophene, the dihedral angles between the two thiophene units, thiophene and phenothiazine are 2.41^{o} and 14.7^{o}, respectively. Obviously, **PH2** possesses a better coplanar configuration than **PH1**. This result indicates a better ICT effect for **PH2** than **PH1** and it is consistent with the absorption properties described above. However, when pyrene group was introduced into the conjugation structure, the torsion angle of the two thiophenes, thiophene and phenothiazine, pyrene and thiophene were 2.15 ^{o}, 14.86 ^{o} and 49.19 ^{o}, respectively.

3.5 Photovoltaic performance of the DSSCs

Fig. 4. exhibits the current-voltage characteristics of the DSSCs fabricated with the three phenothiazine dyes based on an irradiance of simulated AM 1.5G sunlight (100 mW cm^{-2}). The detail photovoltaic parameters of short-circuit photocurrent (J_{sc}), open-circuit photovoltage (V_{oc}), fill factor (FF) and overall conversion efficient (η)

are shown in Table 3. The cell sensitized by **PH1** exhibits the lowest η of 5.64 % with a J_{sc} of 11.2 mA cm^{-2}, a V_{oc} of 730 mV and an *FF* of 0.69. **PH2** exhibits an efficiency of 7.08%, with a J_{sc} of 13.40 mA cm^{-2}, a V_{oc} of 760 mV, and a *FF* of 0.69. In comparison to **PH1**, the higher J_{sc} of **PH2** may be ascribed to the higher molar extinction coefficient. When introducing pyrene into the system, **PH3** exhibits a slight decrease of J_{sc} compared to the other two dyes, which is attributed to the more serious dye aggregation. The good planarity of pyrene might aggravate intermolecular aggregation. In addition, compared with **PH1**, the V_{oc} of **PH2** was improved 30 mV, which is ascribed to the EIMW unit in the architecture. The steric properties and size of the circle chain in the sensitizers may have an obvious impact on the recombination process at the photoelectrode interface in the cells [92]. In addition, the open-circuit voltage (V_{oc}) is similar for **PH2** and **PH3**.

The photoresponse properties of these cells sensitized by **PH1–3** also evaluated by incident photon-to-current conversion efficiency (IPCE) spectra, as shown in Fig. 4a. The three dyes exhibit a broad spectral response range from 300 to 700 nm, indicating that all the three dyes can absorb the visible light convert it into photocurrent efficiently. The IPCE value of **PH2** is over 60% from 400 to 600 nm with a maximum IPCE value of 70% at 550 nm, showing a higher IPCE value than the others. This result in good accordance with the *J*–V (current–voltage) measurements. It is surprised that **PH3** show a good light harvesting ability in absorption spectra (Fig. 2), but lower IPCE values compared to **PH2**. In comparison with **PH2**, the pyene unit was introduced to **PH3,** so the lower IPCE values due to more serious intermecular

aggregation, leading to lower charge injection efficiency [84].

Fig. 4. (a) IPCE spectra and (b) *J*−V curves of these cells based on dyes **PH1-3**.

Fig. 5. *J* − V characteristics of these DSSCs with 1 mM CDCA as a co-adsorbent.

An appropriate amount of chenodeoxycholic acid (CDCA) was added as a co-adsorbent to see if the novel auxiliary donor reduces dye aggregation and charge recombination. The *J* – V curves were measured and shown in Fig. 5, and the specific data were listed in Table 3. The photovoltaic conversion efficiencies were improved for all the three cells when CDCA was added as a co-adsorbent. The efficiency of the cell based on **PH1** was improved about 40% relative to that without CDCA. Such a big improvement indicates that obvious aggregation occurred for **PH1**. However, only about 11% and 20% improvements are for **PH2** and **PH3**, respectively. The less improvement with CDCA, for **PH2** and **PH3** in comparison with **PH1** confirms that the EIMW unit can inhibit dye aggregation to a certain extent.

Table 3. Photovoltaic performance parameters of the DSSCs based on **PH1–3**

3.6 Electrochemical impedance spectra （EIS）

To more explicit the electron recombination in the DSSCs, electrochemical impedance spectroscopy (EIS) was conducted in dark. The Nyquist plots for the DSSCs based on the dyes are shown in Fig. 6 and the detail data shown in Table 4. The first semicircle (R_{ce}) is belonged to the resistance of charge transfer at the counter electrode/electrolyte interface, while the second semicircle (R_{rec}) is belonged to the resistance of charge transfer at the TiO_2/dye/electrolyte interface. Charge transfer

resistance of the counter electrode (R_{ce}) and recombination resistance (R_{rec}) were analyzed by Z-view software using an equivalent circuit. Similar R_{ce} values were obtained in the low frequency range (7.57Ω cm^{-2} for **PH1**, 9.54 Ω cm^{-2} for **PH2**, 10.91 Ω cm^{-2} for **PH3** because of using the same counter electrode and electrolyte at this experiment. The second semicircle (R_{rec}) values for **PH1**, **PH2** and **PH3** are 52.92, 68.29 and 108.4 Ω cm^{-2}, respectively. The electron lifetime (τ_{ct}) of DSSCs were calculated by applying equations of $\tau_{ct} = R_{ct} \times C_{chem}$. The corresponding electron lifetimes for **PH1**, **PH2** and **PH3** are 78, 91 and 156 ms, respectively. The electron lifetime trend is in order of **PH1** < **PH2** < **PH3**, which clearly indicates that the recombination of the injected electron with I^-/I_3^- in the electrolyte can be effectively suppressed by EIMW.

Fig. 6. Electrochemical impedance spectra (Nyquist plot) of the DSSCs measured in the dark.

Table 4. Parameters obtained by fitting the impedance spectra of the DSSCs with **PH1–3**

4. Conclusion

In summary, we designed and synthesized two novel phenothiazine dyes with encapsulated insulated molecular wire as an auxiliary donor, and studied the photoelectric properties of their dye-sensitized solar cells. Compared to **PH1** without EIMW, the rigid circle chain of EIMW of **PH2** can inhibit the dye aggregation greatly, resulting in much higher photovoltage of the cell. In addition, the circle chain plays a

role as a compact layer on the surface of the TiO_2, leading to suppress the charge recombination effectively. The results indicate that it is an effective way to increase the photovoltage and efficiency of the DSSCs by introducing the EIMW into the organic dyes.

ASSOCIATED CONTENT

Supporting Information

Experimental details, ^{1}H NMR, ^{13}C NMR of all of the new compounds and HRMS of **PH1**, **PH2** and **PH3**, spectroscopic data**.**

ACKNOWLEDGMENTS

We are grateful to the National Key Research and Development Program of China (2016YFA0602900), the National Natural Science Foundation of China (21572069, 21772045), and the Natural Science Foundation of Guangdong Province, China (2018B030311008).

NOTES

The authors declare no competing financial interest.

Reference

[1] Hagfeldt, A., G. Boschloo, L. Sun, L. Kloo, and H. Pettersson, Dye-Sensitized Solar Cells, Chemical Reviews 110 (2010) 6595-6663.

[2] Zhang, S., X. Yang, Y. Numata, and L. Han, Highly efficient dye-sensitized solar cells: progress and future challenges, Energy & Environmental Science 6 (2013) 1443.

[3] O'Regan, B. and M. Grätzel, A low-cost, high-efficiency solar cell based on dye-sensitized colloidal TiO2 films, Nature 353 (1991) 737-740.

[4] Yao, Z., M. Zhang, R. Li, L. Yang, Y. Qiao, and P. Wang, A metal-free N-annulated thienocyclopentaperylene dye: power conversion efficiency of 12% for dye-sensitized solar cells, Angewandte Chemie 54 (2015) 5994-8.

[5] Yang, J., P. Ganesan, J. Teuscher, T. Moehl, Y.J. Kim, C. Yi, P. Comte, K. Pei, T.W. Holcombe, M.K. Nazeeruddin, et al., Influence of the Donor Size in D–π–A Organic Dyes for Dye-Sensitized

Solar Cells, J. Am. Chem. Soc. 136 (2014) 5722-5730.

[6] Feng, Q., G. Zhou, and Z.-S. Wang, Varied alkyl chain functionalized organic dyes for efficient dye-sensitized solar cells: Influence of alkyl substituent type on photovoltaic properties, Journal of Power Sources 239 (2013) 16-23.

[7] Liang, M. and J. Chen, Arylamine organic dyes for dye-sensitized solar cells, Chem. Soc. Rev. 42 (2013) 3453.

[8] Mozaffari, S., M.R. Nateghi, and M.B. Zarandi, An overview of the Challenges in the commercialization of dye sensitized solar cells, Renewable and Sustainable Energy Reviews 71 (2017) 675-686.

[9] Petrus, M.L., J. Schlipf, C. Li, T.P. Gujar, N. Giesbrecht, P. Müller-Buschbaum, M. Thelakkat, T. Bein, S. Hüttner, and P. Docampo, Capturing the Sun: A Review of the Challenges and Perspectives of Perovskite Solar Cells, Advanced Energy Materials 7 (2017) 1700264.

[10] Calió, L., S. Kazim, M. Grätzel, and S. Ahmad, Hole-Transport Materials for Perovskite Solar Cells, Angewandte Chemie International Edition 55 (2016) 14522-14545.

[11] Cai, Y., L. Huo, and Y. Sun, Recent Advances in Wide-Bandgap Photovoltaic Polymers, Advanced Materials (2017) 1605437.

[12] Kang, H., G. Kim, J. Kim, S. Kwon, H. Kim, and K. Lee, Bulk-Heterojunction Organic Solar Cells: Five Core Technologies for Their Commercialization, Adv Mater 28 (2016) 7821-7861.

[13] Yao, H., L. Ye, H. Zhang, S. Li, S. Zhang, and J. Hou, Molecular Design of Benzodithiophene-Based Organic Photovoltaic Materials, Chem Rev 116 (2016) 7397-457.

[14] Mathew, S., A. Yella, P. Gao, R. Humphry-Baker, B.F.E. Curchod, N. Ashari-Astani, I. Tavernelli, U. Rothlisberger, M.K. Nazeeruddin, and M. Grätzel, Dye-sensitized solar cells with 13% efficiency achieved through the molecular engineering of porphyrin sensitizers, Nature Chemistry 6 (2014) 242-247.

[15] Yao, Z., H. Wu, Y. Li, J. Wang, J. Zhang, M. Zhang, Y. Guo, and P. Wang, Dithienopicenocarbazole as the kernel module of low-energy-gap organic dyes for efficient conversion of sunlight to electricity, Energy Environ. Sci. 8 (2015) 3192-3197.

[16] Wu, Y., W.H. Zhu, S.M. Zakeeruddin, and M. Gratzel, Insight into D-A-pi-A Structured Sensitizers: A Promising Route to Highly Efficient and Stable Dye-Sensitized Solar Cells, ACS applied materials & interfaces 7 (2015) 9307-18.

[17] <LIZHEN JMCA 2016 efficiency from 5.89% to 9.44% .pdf>.

[18] Zhu, W., Y. Wu, S. Wang, W. Li, X. Li, J. Chen, Z.-s. Wang, and H. Tian, Organic D-A-π-A Solar Cell Sensitizers with Improved Stability and Spectral Response, Advanced Functional Materials 21 (2011) 756-763.

[19] Alagumalai, A., K.M. M, P. Vellimalai, M.C. Sil, and J. Nithyanandhan, Effect of Out-of-Plane Alkyl Group's Position in Dye-Sensitized Solar Cell Efficiency: A Structure-Property Relationship Utilizing Indoline-Based Unsymmetrical Squaraine Dyes, ACS applied materials & interfaces 8 (2016) 35353-35367.

[20] Yang, X., J. Zhao, L. Wang, J. Tian, and L. Sun, Phenothiazine derivatives-based D–π–A and D–A–π–A organic dyes for dye-sensitized solar cells, RSC Advances 4 (2014) 24377.

[21] Chaurasia, S., C.-J. Liang, Y.-S. Yen, and J.T. Lin, Sensitizers with rigidified-aromatics as the conjugated spacers for dye-sensitized solar cells, J. Mater. Chem. C 3 (2015) 9765-9780.

[22] Wang, C.-L., M. Zhang, Y.-H. Hsiao, C.-K. Tseng, C.-L. Liu, M. Xu, P. Wang, and C.-Y. Lin, Porphyrins bearing a consolidated anthryl donor with dual functions for efficient

dye-sensitized solar cells, Energy Environ. Sci. 9 (2016) 200-206.

[23] Cai, N., Y. Wang, M. Xu, Y. Fan, R. Li, M. Zhang, and P. Wang, Engineering of Push-Pull Thiophene Dyes to Enhance Light Absorption and Modulate Charge Recombination in Mesoscopic Solar Cells, Advanced Functional Materials 23 (2013) 1846-1854.

[24] Bai, Y., J. Zhang, D. Zhou, Y. Wang, M. Zhang, and P. Wang, Engineering Organic Sensitizers for Iodine-Free Dye-Sensitized Solar Cells: Red-Shifted Current Response Concomitant with Attenuated Charge Recombination, J. Am. Chem. Soc. 133 (2011) 11442-11445.

[25] Gong, J., K. Sumathy, Q. Qiao, and Z. Zhou, Review on dye-sensitized solar cells (DSSCs): Advanced techniques and research trends, Renewable and Sustainable Energy Reviews 68 (2017) 234-246.

[26] Qi, Q., J. Zhang, S. Das, W. Zeng, J. Luo, J. Zhang, P. Wang, and J. Wu, Push–pull type alkoxy-wrapped N-annulated perylenes for dye-sensitized solar cells, RSC Advances 6 (2016) 81184-81190.

[27] Xie, Y., Y. Tang, W. Wu, Y. Wang, J. Liu, X. Li, H. Tian, and W.H. Zhu, Porphyrin cosensitization for a photovoltaic efficiency of 11.5%: a record for non-ruthenium solar cells based on iodine electrolyte, Journal of the American Chemical Society 137 (2015) 14055-8.

[28] Liu, J., B. Liu, Y. Tang, W. Zhang, W. Wu, Y. Xie, and W.-H. Zhu, Highly efficient cosensitization of D–A–π–A benzotriazole organic dyes with porphyrin for panchromatic dye-sensitized solar cells, J. Mater. Chem. C 3 (2015) 11144-11150.

[29] Hao, Y., Y. Saygili, J. Cong, A. Eriksson, W. Yang, J. Zhang, E. Polanski, K. Nonomura, S.M. Zakeeruddin, M. Grätzel, et al., Novel Blue Organic Dye for Dye-Sensitized Solar Cells Achieving High Efficiency in Cobalt-Based Electrolytes and by Co-Sensitization, ACS Appl. Mater. Interfaces 8 (2016) 32797-32804.

[30] Wu, H.-P., Z.-W. Ou, T.-Y. Pan, C.-M. Lan, W.-K. Huang, H.-W. Lee, N.M. Reddy, C.-T. Chen, W.-S. Chao, C.-Y. Yeh, et al., Molecular engineering of cocktail co-sensitization for efficient panchromatic porphyrin-sensitized solar cells, Energy & Environmental Science 5 (2012) 9843.

[31] Ateş Sönmezoğlu, Ö., S. Akın, B. Terzi, S. Mutlu, and S. Sönmezoğlu, An Effective Approach for High-Efficiency Photoelectrochemical Solar Cells by Using Bifunctional DNA Molecules Modified Photoanode, Advanced Functional Materials 26 (2016) 8776-8783.

[32] Deepankumar, K., A. George, G. Krishna Priya, M. Ilamaran, N.R. Kamini, T.S. Senthil, S. Easwaramoorthi, and N. Ayyadurai, Next Generation Designed Protein as a Photosensitizer for Biophotovoltaics Prepared by Expanding the Genetic Code, ACS Sustainable Chemistry & Engineering 5 (2017) 72-77.

[33] Saranya, K., M. Rameez, and A. Subramania, Developments in conducting polymer based counter electrodes for dye-sensitized solar cells – An overview, Eur. Polym. J. 66 (2015) 207-227.

[34] Elayappan, V., P. Panneerselvam, S. Nemala, K.S. Nallathambi, and S. Angaiah, Influence of PVP template on the formation of porous TiO2 nanofibers by electrospinning technique for dye-sensitized solar cell, Appl. Phys. A 120 (2015) 1211-1218.

[35] Murugadoss, V., N. Wang, S. Tadakamalla, B. Wang, Z. Guo, and S. Angaiah, In situ grown cobalt selenide/graphene nanocomposite counter electrodes for enhanced dye-sensitized solar cell performance, Journal of Materials Chemistry A 5 (2017) 14583-14594.

[36] Saranya, K., A. Subramania, N. Sivasankar, and S. Mallick, Electrospun TiC embedded CNFs as

a low cost platinum-free counter electrode for dye-sensitized solar cell, Mater. Res. Bull. 75 (2016) 83-90.

[37] Saranya, K., N. Sivasankar, and A. Subramania, Microwave-assisted exfoliation method to develop platinum-decorated graphene nanosheets as a low cost counter electrode for dye-sensitized solar cells, RSC Adv. 4 (2014) 36226-36233.

[38] Singh, N., V. Murugadoss, S. Nemala, S. Mallick, and S. Angaiah, Cu2ZnSnSe4 QDs sensitized electrospun porous TiO2 nanofibers as photoanode for high performance QDSC, Solar Energy 171 (2018) 571-579.

[39] Singh, N., Z. Salam, A. Subasri, N. Sivasankar, and A. Subramania, Development of porous TiO 2 nanofibers by solvosonication process for high performance quantum dot sensitized solar cell, Solar Energy Materials and Solar Cells 179 (2018) 417-426.

[40] Salam, Z., E. Vijayakumar, A. Subramania, N. Sivasankar, and S. Mallick, Graphene quantum dots decorated electrospun TiO2 nanofibers as an effective photoanode for dye sensitized solar cells, Solar Energy Materials and Solar Cells 143 (2015) 250-259.

[41] Saranya, K., A. Subramania, and N. Sivasankar, Influence of earth-abundant bimetallic (Fe–Ni) nanoparticle-embedded CNFs as a low-cost counter electrode material for dye-sensitized solar cells, RSC Advances 5 (2015) 43611-43619.

[42] Rameez, M., K. Saranya, A. Subramania, N. Sivasankar, and S. Mallick, Bimetal (Ni–Co) nanoparticles-incorporated electrospun carbon nanofibers as an alternative counter electrode for dye-sensitized solar cells, Appl. Phys. A 122 (2016).

[43] Zhang, Y., Y. Zhang, Z. Wang, M. Liang, D. Jia, Q. Wu, and S. Xue, Effects of different alkyl chains on the performance of dye-sensitized solar cells with different electrolytes, Journal of Power Sources 253 (2014) 167-176.

[44] Murugadoss, V., S. Arunachalam, V. Elayappan, and S. Angaiah, Development of electrospun PAN/CoS nanocomposite membrane electrolyte for high-performance DSSC, Ionics (2018).

[45] E, V., S. A, Z. Fei, and P.J. Dyson, Effect of 1-butyl-3-methylimidazolium iodide containing electrospun poly(vinylidene fluoride-co-hexafluoropropylene) membrane electrolyte on the photovoltaic performance of dye-sensitized solar cells, J. Appl. Polym. Sci. 132 (2015) n/a-n/a.

[46] Elayappan, V., V. Murugadoss, S. Angaiah, Z. Fei, and P.J. Dyson, Development of a conjugated polyaniline incorporated electrospun poly(vinylidene fluoride-co-hexafluoropropylene) composite membrane electrolyte for high performance dye-sensitized solar cells, J. Appl. Polym. Sci. 132 (2015) n/a-n/a.

[47] Vijayakumar, E., A. Subramania, Z. Fei, and P.J. Dyson, High-performance dye-sensitized solar cell based on an electrospun poly(vinylidene fluoride-co-hexafluoropropylene)/cobalt sulfide nanocomposite membrane electrolyte, RSC Advances 5 (2015) 52026-52032.

[48] Meier, H., Z.-S. Huang, and D. Cao, Double D–π–A branched dyes – a new class of metal-free organic dyes for efficient dye-sensitized solar cells, J. Mater. Chem. C 5 (2017) 9828-9837.

[49] Cao, D., J. Peng, Y. Hong, X. Fang, L. Wang, and H. Meier, Enhanced Performance of the Dye-Sensitized Solar Cells with Phenothiazine-Based Dyes Containing Double D−A Branches, Org. Lett. 13 (2011) 1610-1613.

[50] Huang, Z.-S., H. Meier, and D. Cao, Phenothiazine-based dyes for efficient dye-sensitized solar cells, Journal of Materials Chemistry C 4 (2016) 2404-2426.

[51] Zhang, C., S. Wang, and Y. Li, Phenothiazine organic dyes containing dithieno[3,2-b:2′,3′-d]pyrrole (DTP) units for dye-sensitized solar cells, Solar Energy 157 (2017) 94-102.

[52] Wan, Z., C. Jia, J. Zhang, Y. Duan, Y. Lin, and Y. Shi, Triphenylamine-based starburst dyes with carbazole and phenothiazine antennas for dye-sensitized solar cells, Journal of Power Sources 199 (2012) 426-431.

[53] Chen, S.-G., H.-L. Jia, X.-H. Ju, and H.-G. Zheng, The impact of adjusting auxiliary donors on the performance of dye-sensitized solar cells based on phenothiazine D-D-π-A sensitizers, Dyes and Pigments 146 (2017) 127-135.

[54] Yang, W., D. Cao, H. Zhang, X. Yin, X. Liao, J. Huang, G. Wu, L. Li, and Y. Hong, Dye-sensitized solar cells based on (D−π−A) 3 L 2 phenothiazine dyes containing auxiliary donors and flexible linkers with different length of carbon chain, Electrochimica Acta 283 (2018) 1732-1741.

[55] Wang, S., H. Wang, J. Guo, H. Tang, and J. Zhao, Influence of the terminal electron donor in D–D–π–A phenothiazine dyes for dye-sensitized solar cells, Dyes and Pigments 109 (2014) 96-104.

[56] Yang, C.-J., Y.J. Chang, M. Watanabe, Y.-S. Hon, and T.J. Chow, Phenothiazine derivatives as organic sensitizers for highly efficient dye-sensitized solar cells, Journal of Materials Chemistry 22 (2012) 4040.

[57] Wang, S., R. Yang, J. Guo, and G. Li, Phenothiazine organic dyes with the cone-shaped structural: Broad photoresponse and limitations on short-circuit photocurrent density in dye-sensitized solar cells, Synthetic Metals 215 (2016) 184-193.

[58] Hua, Y., S. Chang, J. He, C. Zhang, J. Zhao, T. Chen, W.-Y. Wong, W.-K. Wong, and X. Zhu, Molecular Engineering of Simple Phenothiazine-Based Dyes To Modulate Dye Aggregation, Charge Recombination, and Dye Regeneration in Highly Efficient Dye-Sensitized Solar Cells, Chemistry - A European Journal 20 (2014) 6300-6308.

[59] Eom, Y.K., I.T. Choi, S.H. Kang, J. Lee, J. Kim, M.J. Ju, and H.K. Kim, Thieno[3,2-b][1]benzothiophene Derivative as a New π-Bridge Unit in D-π-A Structural Organic Sensitizers with Over 10.47% Efficiency for Dye-Sensitized Solar Cells, Advanced Energy Materials 5 (2015) 1500300.

[60] Gao, H.-H., X. Qian, W.-Y. Chang, S.-S. Wang, Y.-Z. Zhu, and J.-Y. Zheng, Oligothiophene-linked D– π –A type phenothiazine dyes for dye-sensitized solar cells, Journal of Power Sources 307 (2016) 866-874.

[61] Yang, Z., C. Liu, C. Shao, C. Lin, and Y. Liu, First-Principles Screening and Design of Novel Triphenylamine-Based D–π–A Organic Dyes for Highly Efficient Dye-Sensitized Solar Cells, The Journal of Physical Chemistry C 119 (2015) 21852-21859.

[62] Zang, X.-F., Z.-S. Huang, H.-L. Wu, Z. Iqbal, L. Wang, H. Meier, and D. Cao, Molecular design of the diketopyrrolopyrrole-based dyes with varied donor units for efficient dye-sensitized solar cells, Journal of Power Sources 271 (2014) 455-464.

[63] Más-Montoya, M. and R.A.J. Janssen, The Effect of H- and J-Aggregation on the Photophysical and Photovoltaic Properties of Small Thiophene-Pyridine-DPP Molecules for Bulk-Heterojunction Solar Cells, Advanced Functional Materials 27 (2017) 1605779.

[64] Zhang, L. and J.M. Cole, Dye aggregation in dye-sensitized solar cells, J. Mater. Chem. A (2017).

[65] Bisht, R., K.M. M, A.K. Singh, and J. Nithyanandhan, Panchromatic Sensitizer for Dye-Sensitized Solar Cells: Unsymmetrical Squaraine Dyes Incorporating Benzodithiophene pi-Spacer with Alkyl Chains to Extend Conjugation, Control the Dye Assembly on TiO2, and Retard Charge Recombination, J Org Chem 82 (2017) 1920-1930.

[66] Lu, Z., M. Liang, P. Dai, K. Miao, C. Zhang, Z. Sun, and S. Xue, A Strategy for Enhancing the Performance of Borondipyrromethene Dye-Sensitized Solar Cells, The Journal of Physical Chemistry C 120 (2016) 25657-25667.

[67] Tang, Y., Y. Wang, X. Li, H. Agren, W.H. Zhu, and Y. Xie, Porphyrins Containing a Triphenylamine Donor and up to Eight Alkoxy Chains for Dye-Sensitized Solar Cells: A High Efficiency of 10.9%, ACS applied materials & interfaces 7 (2015) 27976-85.

[68] Lee, Y.H., R.K. Chitumalla, B.Y. Jang, J. Jang, S. Thogiti, and J.H. Kim, Alkyl chain length dependence of the charge-transfer, recombination and electron diffusion length on the photovoltaic performance in double donor-acceptor-based organic dyes for dye sensitized solar cells, Dyes and Pigments 133 (2016) 161-172.

[69] Su, J., Y. Chen, Y. Wu, R.P. Ghimire, Y. Xu, X. Liu, Z. Wang, and M. Liang, New triarylamine organic dyes containing the 9-hexyl-2-(hexyloxy)-9H-carbazole for dye-sensitized solar cells, Electrochimica Acta 254 (2017) 191-200.

[70] Jia, H.-L., M.-D. Zhang, W. Yan, X.-H. Ju, and H.-G. Zheng, Effects of structural optimization on the performance of dye-sensitized solar cells: spirobifluorene as a promising building block to enhance Voc, J. Mater. Chem. A 4 (2016) 11782-11788.

[71] Li, X., X. Zhang, J. Hua, and H. Tian, Molecular engineering of organic sensitizers with o,p-dialkoxyphenyl-based bulky donors for highly efficient dye-sensitized solar cells, Mol. Syst. Des. Eng. (2017).

[72] Tian, G., S. Cai, X. Li, H. Ågren, Q. Wang, J. Huang, and J. Su, A new D–A–π–A type organic sensitizer based on substituted dihydroindolo [2,3-b] carbazole and DPP unit with a bulky branched alkyl chain for highly efficient DSCs, J. Mater. Chem. A 3 (2015) 3777-3784.

[73] Islam, A., T. Swetha, M.R. Karim, M. Akhtaruzzaman, L. Han, and S.P. Singh, Tuning of spectral response by co-sensitization in black-dye based dye-sensitized solar cell, physica status solidi (a) 212 (2015) 651-656.

[74] Luo, J., Z. Wan, C. Jia, Y. Wang, X. Wu, and X. Yao, Co-sensitization of Dithiafulvenyl-Phenothiazine Based Organic Dyes with N719 for Efficient Dye-Sensitized Solar Cells, Electrochimica Acta 211 (2016) 364-374.

[75] <J. Phys. Chem. C, Vol. 113, No. 23, 2009.pdf>.

[76] Rao, S.-J., Q. Zhang, J. Mei, X.-H. Ye, C. Gao, Q.-C. Wang, D.-H. Qu, and H. Tian, One-pot synthesis of hetero[6]rotaxane bearing three different kinds of macrocycle through a self-sorting process, Chem. Sci. 8 (2017) 6777-6783.

[77] Cao, Z.-Q., Y.-C. Wang, A.-H. Zou, G. London, Q. Zhang, C. Gao, and D.-H. Qu, Reversible switching of a supramolecular morphology driven by an amphiphilic bistable [2]rotaxane, Chem. Commun. 53 (2017) 8683-8686.

[78] Li, Z., G. Liu, W. Xue, D. Wu, Y.-W. Yang, J. Wu, S.H. Liu, J. Yoon, and J. Yin, Construction of Hetero[n]rotaxanes by Use of Polyfunctional Rotaxane Frameworks, The Journal of Organic Chemistry 78 (2013) 11560-11570.

[79] Liu, J., X. Yang, A. Islam, Y. Numata, S. Zhang, N.T. Salim, H. Chen, and L. Han, Efficient metal-free sensitizers bearing circle chain embracing π-spacers for dye-sensitized solar cells, Journal of Materials Chemistry A 1 (2013) 10889.

[80] Saritha, G., J.J. Wu, and S. Anandan, Modified pyrene based organic sensitizers with thiophene-2-acetonitrile as π-spacer for dye sensitized solar cell applications, Organic Electronics 37 (2016) 326-335.

[81] Taratula, O., J. Rochford, P. Piotrowiak, E. Galoppini, R.A. Carlisle, and G.J. Meyer, Pyrene-Terminated Phenylenethynylene Rigid Linkers Anchored to Metal Oxide Nanoparticles, The Journal of Physical Chemistry B 110 (2006) 15734-15741.

[82] Nagarajan, B., S. Kushwaha, R. Elumalai, S. Mandal, K. Ramanujam, and D. Raghavachari, Novel ethynyl-pyrene substituted phenothiazine based metal free organic dyes in DSSC with 12% conversion efficiency, J. Mater. Chem. A 5 (2017) 10289-10300.

[83] Chen, C., J.-Y. Liao, Z. Chi, B. Xu, X. Zhang, D.-B. Kuang, Y. Zhang, S. Liu, and J. Xu, Metal-free organic dyes derived from triphenylethylene for dye-sensitized solar cells: tuning of the performance by phenothiazine and carbazole, Journal of Materials Chemistry 22 (2012) 8994.

[84] Huang, Z.-S., H.-L. Feng, X.-F. Zang, Z. Iqbal, H. Zeng, D.-B. Kuang, L. Wang, H. Meier, and D. Cao, Dithienopyrrolobenzothiadiazole-based organic dyes for efficient dye-sensitized solar cells, J. Mater. Chem. A 2 (2014) 15365-15376.

[85] Iqbal, Z., W.-Q. Wu, H. Zhang, L. Han, X. Fang, L. Wang, D.-B. Kuang, H. Meier, and D. Cao, Influence of spatial arrangements of π-spacer and acceptor of phenothiazine based dyes on the performance of dye-sensitized solar cells, Organic Electronics 14 (2013) 2662-2672.

[86] Chen, T., L. Qiu, Z. Cai, F. Gong, Z. Yang, Z. Wang, and H. Peng, Intertwined Aligned Carbon Nanotube Fiber Based Dye-Sensitized Solar Cells, Nano Lett. 12 (2012) 2568-2572.

[87] Feng, S., Q.-S. Li, T.A. Niehaus, and Z.-S. Li, Effects of different electron donating groups on dye regeneration and aggregation in phenothiazine-based dye-sensitized solar cells, Organic Electronics 42 (2017) 234-243.

[88] Sugiyasu, K., Y. Honsho, R.M. Harrison, A. Sato, T. Yasuda, S. Seki, and M. Takeuchi, A Self-Threading Polythiophene: Defect-Free Insulated Molecular Wires Endowed with Long Effective Conjugation Length, J. Am. Chem. Soc. 132 (2010) 14754-14756.

[89] Steemers, L., M.J. Wanner, A.W. Ehlers, H. Hiemstra, and J.H. van Maarseveen, A Short Covalent Synthesis of an All-Carbon-Ring [2]Rotaxane, Org. Lett. 19 (2017) 2342-2345.

[90] <Chem. Mater., Vol. 20, No. 5, 2008 1833.pdf>.

[91] Luo, J., M. Xu, R. Li, K.W. Huang, C. Jiang, Q. Qi, W. Zeng, J. Zhang, C. Chi, P. Wang, et al., N-annulated perylene as an efficient electron donor for porphyrin-based dyes: enhanced light-harvesting ability and high-efficiency Co(II/III)-based dye-sensitized solar cells, Journal of the American Chemical Society 136 (2014) 265-72.

[92] Liu, P., W. Sharmoukh, B. Xu, Y.Y. Li, G. Boschloo, L. Sun, and L. Kloo, Novel and Stable D–A–π–A Dyes for Efficient Solid-State Dye-Sensitized Solar Cells, ACS Omega 2 (2017) 1812-1819.

Figure and Table Captions

Table 1. Photophysical and electrochemical properties of the dyes

Table 2. The computed energy levels and the spatial distribution of the frontier molecular orbitals of the dyes

Table 3. Photovoltaic performance parameters of the DSSCs based on **PH1–3**

Table 4. Parameters obtained by fitting the impedance spectra of the DSSCs with **PH1–3**

Scheme 1. Synthesis routes of dyes **PH1–3**.

Fig. 1. Chemical structures of the sensitizers (**PH1**, **PH2** and **PH3**).

Fig. 2. The UV-Vis absorption spectra of the dyes in solution (a) and the absorption spectra of these dyes adsorbed on TiO_2 films (b).

Fig. 3. Cyclic voltammograms (a) and Schematic energy diagrams of these dyes (b).

Fig. 4. (a) IPCE spectra and (b) J−V curves of the DSSCs based on dyes **PH1-3**.

Fig. 5. J − V characteristics of the DSSCs with 1 mM CDCA as a co-adsorbent.

Fig. 6. Electrochemical impedance spectra (Nyquist plot) of the DSSCs measured in the dark.

Table 1. Photophysical and electrochemical properties of the dyes

Dye	λ_{max}/nm[a]	ε/M^{-1} cm^{-1}	λ_{max}/nm [b]	$E_{0\text{-}0}$/eV[d]	HOMO[c]	LUMO[e]
PH1	493	21500	466	2.15	0.94	–1.21
PH2	506	23900	492	2.16	0.95	–1.21
PH3	508	28900	466	2.24	1.14	–1.10

[a] Absorption maximum measured in CH_2Cl_2 (1×10^{-5} M). [b] Absorption maximum peak of dye adsorbed on TiO_2. [c] Oxidation potential measured in CH_3CN containing 0.1 M $(n\text{-}C_4H_9)_4NPF_6$ with a scan rate of 50 mVs^{-1} (vs. a normal hydrogen electrode (NHE)). [d] Zero–zero band gap was determined from the intersection of the normalized absorption and emission spectra. [e] LUMO = HOMO – $E_{0\text{-}0}$.

Table 2. The computed energy levels and the spatial distribution of the frontier molecular orbitals of the dyes

	PH1	PH2	PH3
optimized geometries	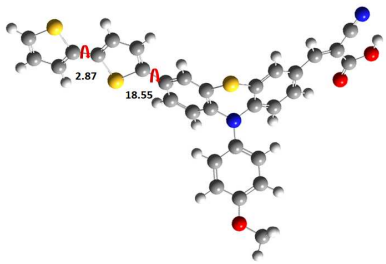	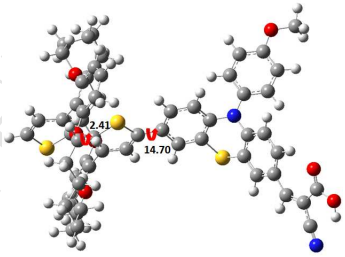	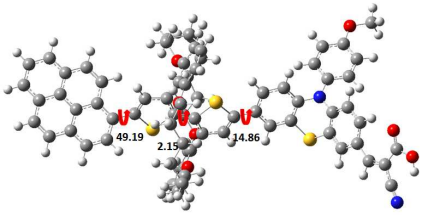
HOMO	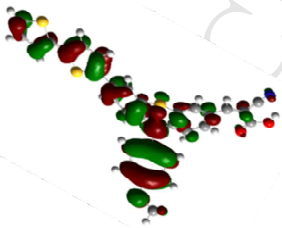	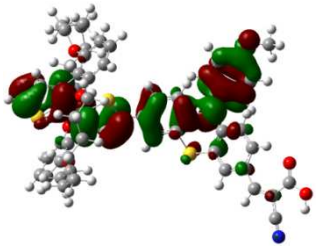	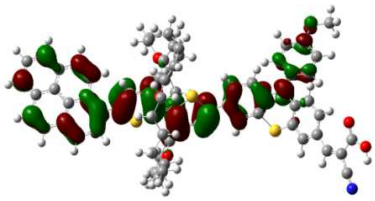
LUMO	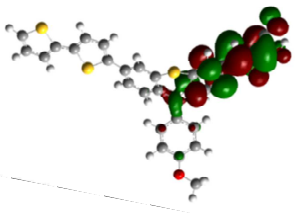	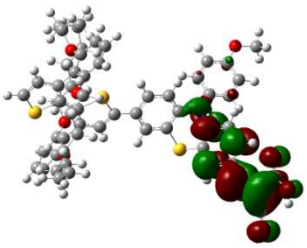	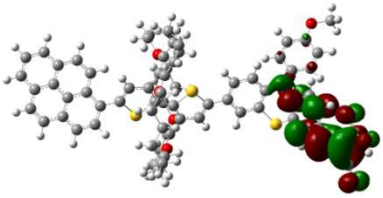

Table 3. Photovoltaic performance parameters of the DSSCs based on **PH1–3**

Dye	J_{sc} (mA cm^{-2})	V_{oc} (V)	*FF*	η (%)
PH1	11.20	0.73	0.69	5.64
PH2	13.40	0.76	0.69	7.08
PH3	12.68	0.77	0.67	6.51
PH1+CDCA	16.08	0.74	0.67	7.92
PH2+CDCA	14.79	0.78	0.69	7.88
PH3+CDCA	14.48	0.79	0.69	7.85
N719	16.41	0.68	0.68	7.61

The electrolyte solution is composed of 0.6 M 1-metyl-3-propylimidazoliumiodide (PMII), 0.05 M LiI, 0.10 M guanidiniumthiocyanate, 0.03 M I_2 and 0.5 M tert-butylpridine in acetonitrile/valeronitrile (85 : 15) was injected from a hole made on the counter electrode into the space between the sandwiched cells. The active area of those dyes coated on TiO_2 was 0.16 cm^2. The photoanodes were immersed in a 3.0×10^{-4} M solution of the dyes for 24 h (The dye solutions were prepared in the mixture of CH_3CN/tert-BuOH = 1:1).

Table 4. Parameters obtained by fitting the impedance spectra of the DSSCs with **PH1–3**

Dye	R_{ce} (Ω cm^{-2})	R_{rec} (Ω cm^{-2})	CPE (μ F)	τ (ms)
PH1	7.57	52.92	1477	78
PH2	9.54	68.29	1336	91
PH3	10.91	108.4	1441	156

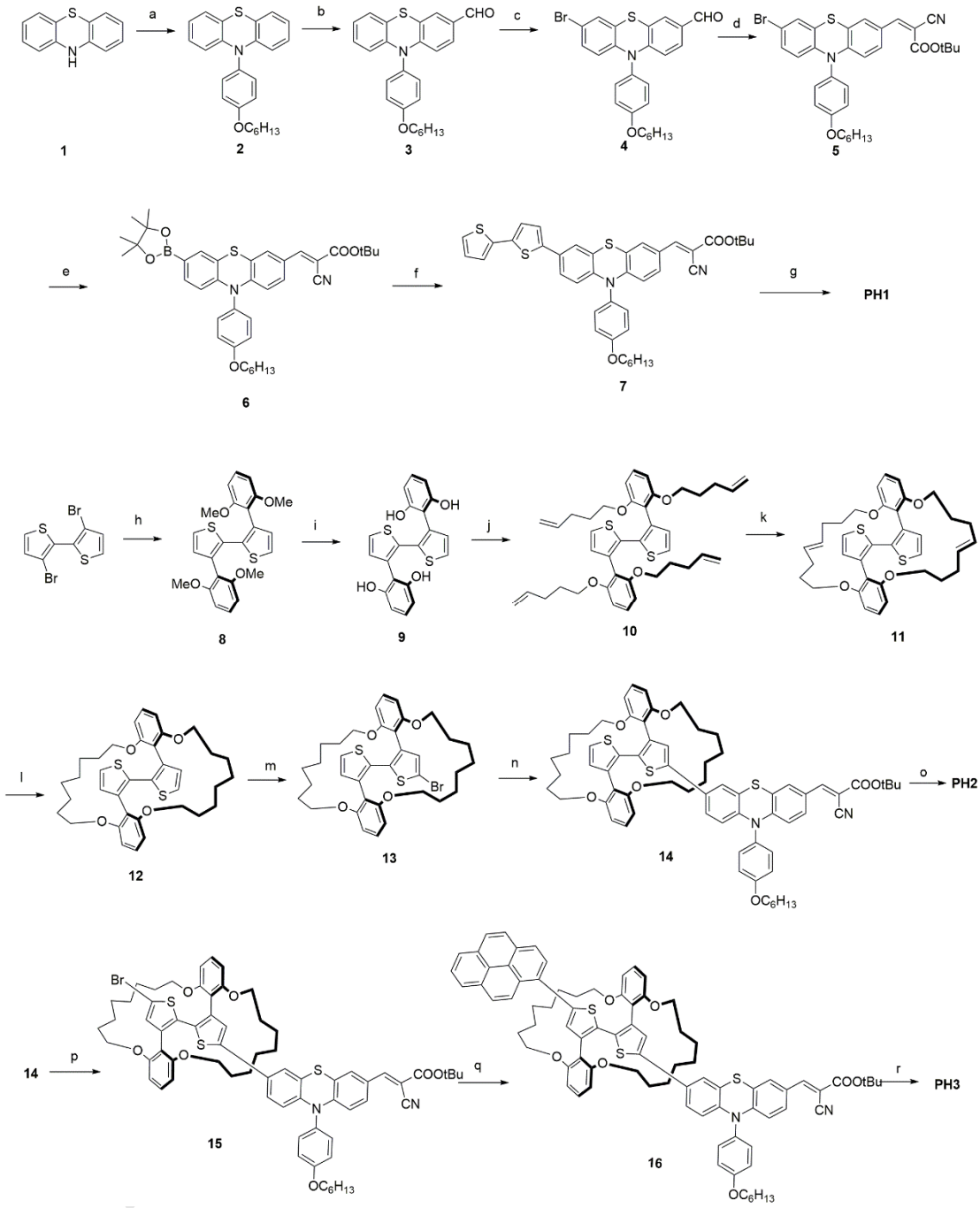

Scheme 1.

Synthesis routes of dyes **PH1–3**. a.1-(Hexyloxy)-4-iodobenzene, $Pd_2(dba)_3$, t-BuOK, $P(t\text{-}Bu)_3$, toluene, 110 ^oC, 24 h, 78%; b. $POCl_3$, DMF, 1,2-dichloroethane, 60 ^oC, 72%; c. NBS, THF, rt, 8 h, 85.5%; d. NH_4AC, CH_3COOH, tert-butyl cyanoacetate, toluene, 130 ^oC, 4 h, 93.9%; e. KOAC, $Pd(dppf)_2Cl_2$, bis(pinacolato)diboron, 1,4-dioxane, 95 ^oC, 18 h, 64%; f. 5-bromo-2,2'-bithiophene， $Pd(PPh_3)_4$, Na_2CO_3, CH_3CH_2OH/H_2O,

toluene, 18 h, 90 ^{o}C, 67.5%; g. CF_3COOH, rt, 3h, 91%; h. (2,6-dimethoxyphenyl)boronic acid, $Pd_2(dba)_3$, s-Phos, K_3PO_4, toluene, 105 ^{o}C, 18 h, 75%; i. BBr_3, CH_2Cl_2, 0 ^{o}C, 2 h, 68%; j. Cs_2CO_3, DMSO, 5-bromo-1-pentene, 100 ^{o}C, 10 h, 88%; k. 2nd generation Grubbs catalyst, CH_2Cl_2, 40 ^{o}C, 3 h, 59.6%; l. Pd/C, CH_2Cl_2/CH_3OH, H_2, 5h, 35 ^{o}C, quantitatively; m. NBS, THF, 0 ^{o}C, 5min, 82%; n. Compound **6**, $Pd(PPh_3)_4$, Na_2CO_3, CH_3CH_2OH/H_2O, toluene, 18 h, 90 ^{o}C, 52%; o. CF_3COOH, rt, 3 h, 90%; p. NBS, THF, 0 ^{o}C, 6 h, 52%; q. 4,4,5,5-tetramethyl-2-(pyren-1-yl)-1,3,2-dioxaborolane, $Pd(PPh_3)_4$, Na_2CO_3, CH_3CH_2OH/H_2O, toluene, 18 h, 90 ^{o}C, 62%; r. CF_3COOH, rt, 3 h, 87%.

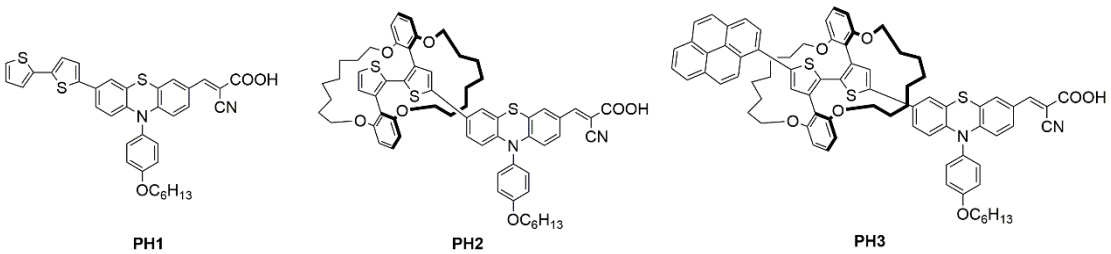
PH1
PH2
PH3

Fig. 1.

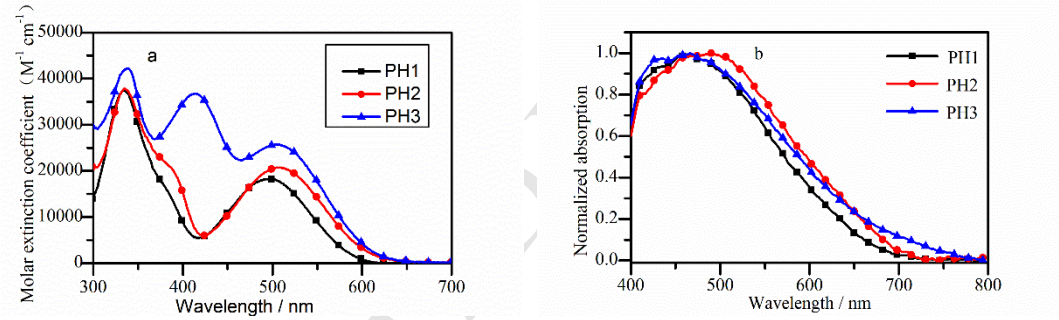
a
PH1
PH2
PH3
Molar extinction coefficient (M-1 cm-1)
Wavelength / nm
b
PH1
PH2
PH3
Normalized absorption
Wavelength / nm

Fig. 2

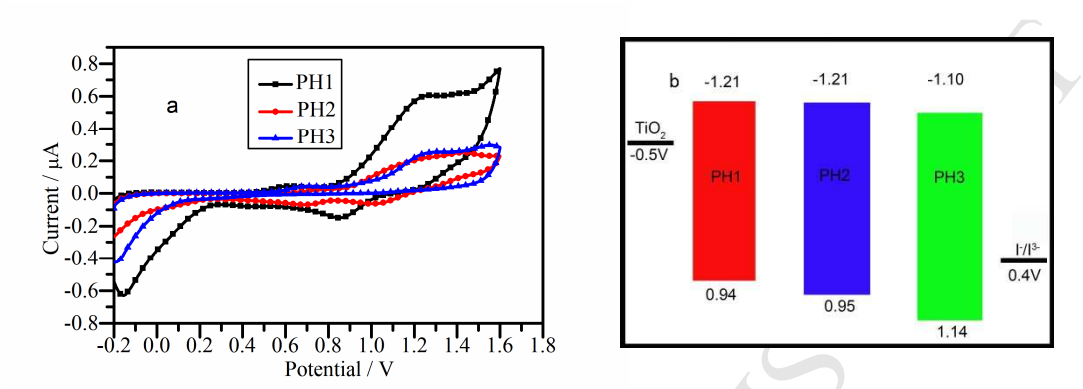
a
PH1
PH2
PH3
Current / μA
Potential / V
b
-1.21
-1.21
-1.10
TiO2
-0.5V
PH1
PH2
PH3
I-/I3-
0.4V
0.94
0.95
1.14

Fig. 3

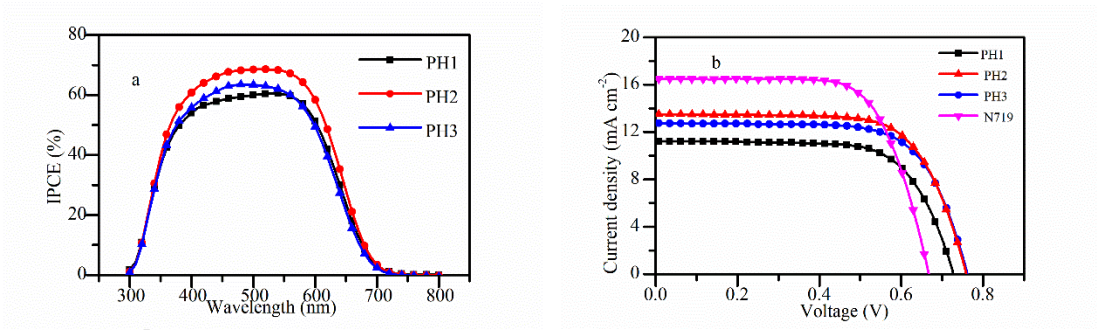
a
PH1
PH2
PH3
IPCE (%)
Wavelength (nm)
b
PH1
PH2
PH3
N719
Current density (mA cm-2)
Voltage (V)

Fig.4

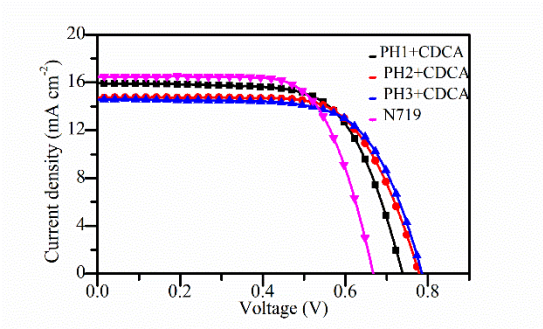

Fig. 5

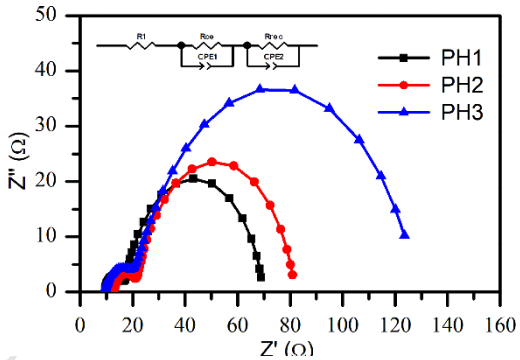

Fig. 6

Graphical Abstract